analytical chemistry

Article

pubs.acs.org/ac

Highly Time-Resolved Imaging of Combustion and Pyrolysis Product Concentrations in Solid Fuel Combustion: NO Formation in a Burning Cigarette

Ralf Zimmermann,*[,†,‡] Romy Hertz-Schünemann,[†,§] Sven Ehlert,[†,§] Chuan Liu,[∥] Kevin McAdam,[∥] Richard Baker,[∥,#] and Thorsten Streibel[†,‡]

[†]Joint Mass Spectrometry Centre, Institute of Chemistry, Chair of Analytical Chemistry, University of Rostock, Rostock, D-18057, Germany

[‡]Joint Mass Spectrometry Centre, Cooperation Group "Comprehensive Molecular Analytics", Helmholtz Zentrum Muenchen, Neuherberg, D-85764, Germany

[§]Photonion GmbH, Schwerin, 19061, Germany

[∥]GR&D, British American Tobacco, Southampton, SO15 8TL, United Kingdom

Supporting Information

ABSTRACT: The highly dynamic, heterogeneous combustion process within a burning cigarette was investigated by a miniaturized extractive sampling probe (microprobe) coupled to photoionization mass spectrometry using soft laser single photon ionization (SPI) for online real-time detection of molecular ions of combustion and pyrolysis products. Research cigarettes smoked by a smoking machine are used as a reproducible model system for solid-state biomass combustion, which up to now is not addressable by current combustion-diagnostic tools. By combining repetitively recorded online measurement sequences from different sampling locations in an imaging approach, highly time- and space-resolved quantitative distribution maps of, e.g., nitrogen monoxide, benzene, and oxygen concentrations were obtained at a near microscopic level. The obtained quantitative distribution maps represent a time-resolved, movie-like imaging of the respective compound's formation and destruction zones in the various combustion and pyrolysis regions of a cigarette during puffing. Furthermore, spatially resolved kinetic data were ascertainable. The here demonstrated methodology can also be applied to various heterogenic combustion/pyrolysis or reaction model systems, such as fossil- or biomass-fuel pellet combustion or to a positional resolved analysis of heterogenic catalytic reactions.

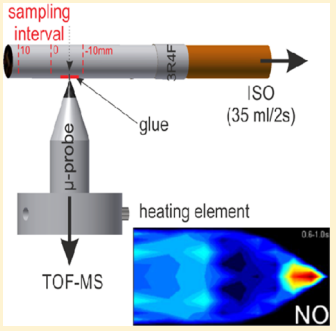

Combustion and pyrolysis are complex chemical and dynamic processes, which are not yet well understood in complete detail.[1−3] Progress in combustion research is often led by development of new analytical technologies and model systems allowing reproducible characterization of relevant physical and chemical processes.[4,5] For example, model flames such as premixed fuel/oxidant gas burners have been used in various studies.[6,7] Laser-based techniques allow the imaging of small molecule/radical concentrations or distributions of soot particles in gas phase combustion systems or internal combustion engines.[8−11] Extractive probing followed by mass spectrometry (MS) is a well-elaborated approach for the detection of combustion products.[12,13] Probes such as quartz skimmers have been used to analyze neutral, radical, and ionic chemical species in model flames by MS.[10] Flame and exhaust composition in industrial combustion processes such as waste incineration plants have been addressed by MS as well.[13,14]

Comparable fundamental studies on the combustion zone of solid fuel combustion, however, are challenging. The solid fuel combustion process exhibits different phases. In the initial preheating or dry distillation phase, the fuel dehydrates and releases organic pyrolysis products. When the temperature reaches the flash point or ignition temperature, flaming or gaseous combustion starts and this phase continues until the vaporizable fuel is depleted. In the final solid char combustion phase, the residual carbon burns-off in an oxygen diffusion-limited manner. During each of the phases, specific inorganic and organic pyrolysis and combustion products are released and formed.

The irreproducible character of solid fuel combustion, however, renders the generation of well-characterized standard "burners" challenging.The burning of tobacco when a cigarette is puffed represents a solid-state combustion model system in which the above-mentioned phases are occurring in a rapidly changing manner. To characterize cigarette emissions, which is in the interest of public health and regulatory activities,[15,16] standard machine-smoking protocols (e.g., ISO-3308) have been developed.[17] This methodology allows for the controlled combustion of tobacco in cigarettes in a highly repeatable

Received: September 18, 2014
Accepted: December 13, 2014
Published: January 12, 2015

DOI: 10.1021/ac503512a
Anal. Chem. 2015, 87, 1711−1717

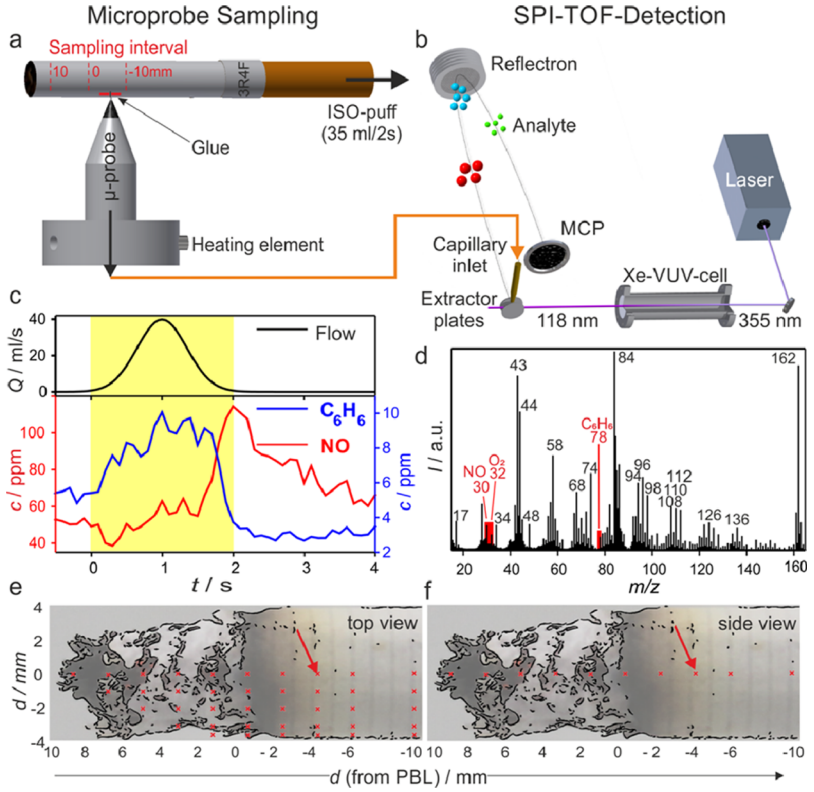

Figure 1. Depiction of the extractive μ-probe sampling as well as its coupling to single photon ionization time-of-flight mass spectrometry (μ-probe-SPI-TOFMS) for the spatially resolved analysis of combustion gases in a burning cigarette. (a) Representation of the μ-probe−cigarette arrangement. The capillary at the tip of the heated μ-probe body is penetrating into the cigarette rod. The sampling interval is indicated. (b) The gases sampled via the μ-probe are led by a heated transfer capillary into the ion source of the photoionization mass spectrometer. Analytes are softly ionized by 118 nm laser pulses and detected in the time-of-flight MS. (c) Flow profile of a single puff taken by a smoking machine according to the ISO protocol and the online measured concentration profiles of NO and benzene during the third puff from the sampling position depicted in (e/f) by a red arrow. (d) Typical corresponding averaged SPI mass spectrum of the combustion gases. The analytes discussed in detail (O_2, NO, benzene) are assigned. The assignment of the other indicated m/z values is given in Table 1 in the Supporting Information. (e) Penetration depths of the μ-probe sampling experiments performed in the sampling interval (top view as in a). (f) Sampling capillary introduction positions of the μ-probe sampling experiments performed in the specified interval (side view).

manner.[18] Combustion and pyrolysis processes occurring during cigarette smoking are highly transient due to the alternating cycles of puffing and smoldering. Thus, many mechanistic studies on tobacco combustion have been reported.[19,20,12,21] In this study, we have applied photoionization mass spectrometry (single-photon ionization time-of-flight mass spectrometry, SPI-TOF-MS[22−24]) coupled with a newly designed, optimized microprobe sampling device ("μ-probe") to conduct high resolution time and spatially resolved mapping of combustion and pyrolysis products within a burning cigarette during the course of a single cigarette puff.

EXPERIMENTAL SECTION

In Figure 1a,b, the setup of the μ-probe-sampling-photoionization mass spectrometer system for mapping combustion byproducts is depicted. Photographs of the setup are shown in Figure S1 (Supporting Information). In principle, the μ-probe represents a sampling capillary by which a small sampling flow from a local environment can be drawn into a mass analyzer. It consists of a steel capillary of 200 μm inner diameter with a protruding tip of 0.5−4 mm,[25] set inside a conically tapered, heated aluminum holder, which is mounted on the x−y precision positioning stage. The holder is connected to a cold-spot-free flexible heating tube. A stainless steel capillary (inner diameter, 270 μm; total length, 2 m) is connected via a union holder to the μ-probe capillary and runs through the heating tube directly to the inlet needle of the photoionization mass spectrometer ion source. It acts as a deactivated transfer line and pressure restrictor between the μ-probe sampling spot in the cigarette and the vacuum of the ion source. The μ-probe body and the transfer line are heated to 270 and 280 °C, respectively. The tip of the stainless steel sampling capillary of the μ-probe is heated to 120 °C by heat conduction from the μ-probe body. The rather low temperature of the μ-probe avoids local preheating of tobacco and quenches the high-temperature combustion chemistry when the hot combustion gases are sampled during the transient puff.[26] However, along the sampling path, the temperature is gradually increasing while the pressure is dropping from ambient conditions to the ion source vacuum ($\sim 10^{-4}$ mbar). In conjunction with the relatively large linear flow in the capillary (>1 m/s), this secures a nearly memory and retention free transfer of molecules with molecular weights larger than ~180 m/z.

The μ-probe was mounted on a precision x−y displacement unit in order to accurately define the linear positioning. The x-direction proceeds along the length of the cigarette rod. The y-direction describes the depth in radial direction, where the tip of the μ-probe is located. All in all, 10 positions along the cigarette rod (x-direction) in the region of 3.0−23.0 mm from the front tip of the cigarette have been chosen. For every

DOI: 10.1021/ac503512a
Anal. Chem. 2015, 87, 1711−1717

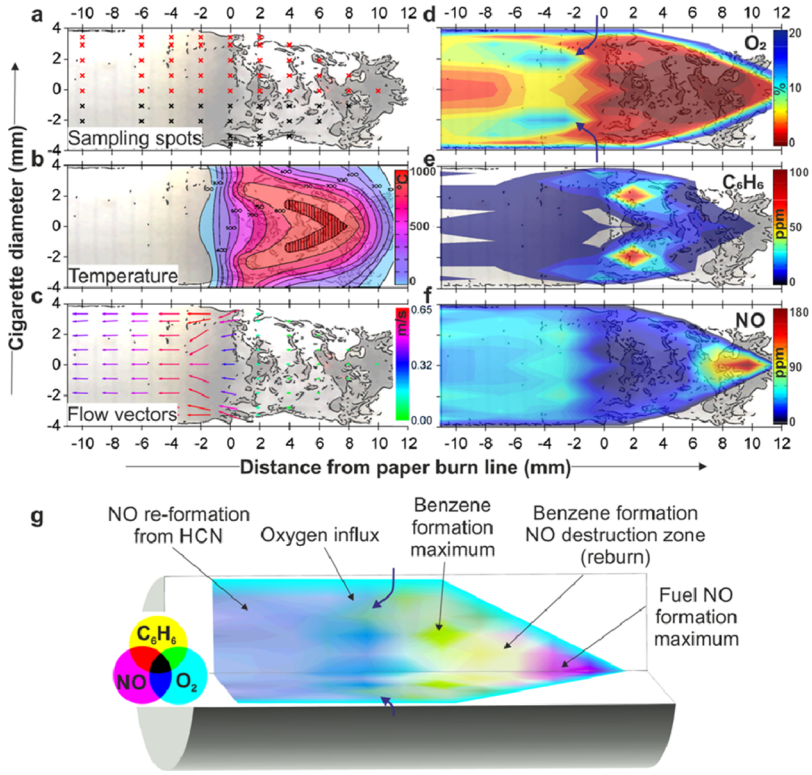

Figure 2. (a) Lit cigarette showing the 40 sampling spots for μ-probe sampling and mass spectral recording of the mapping information (red crosses). Each sampling spot was addressed 4 times for averaging. The black crosses mirrored spots for data analysis. The paper burn line (PBL) in the middle of the 3rd ISO puff is highly reproducible during the middle of the third puff and represents the reference (i.e., PBL = 0). (b) Color-coded temperature distribution during the middle of a puff (after ref 33). (c) Vectors representing linear flow speed and direction at the sampling points during middle of a puff (after ref 34). (d) Color-coded concentration maps of the oxygen (O_2, m/z 32) concentrations after the obtained μ-probe-SPI-MS data during the middle of the puff. (e) Color-coded concentration maps of the benzene (C_6H_6, m/z 78) concentrations after the obtained μ-probe-SPI-MS data during the middle of the puff. (f) Color-coded concentration maps of the nitrogen monoxide (NO, m/z 30) concentrations after the obtained μ-probe-SPI-MS data during the middle of the puff. (g) Due to the rotational symmetry of the cigarette, the measured concentration distribution map during a puff describe the three-dimensional distribution in the cigarette rod.

position in the x-direction, up to five depths-positionings were sampled to a precision of ±250 μm (y-direction, the chosen penetration depths into the cigarette rod were 4.0, 3.0, 2.0, 1.0, and 0.05 mm, respectively). The μ-probe injection hole in the cigarette paper was sealed by a small quantity of starch-based glue, which normally is used to seal the cigarette paper seam.

The sampled volatile and semivolatile smoke components (~15 μL/s) were analyzed online by SPI-TOF-MS in real-time. The SPI-TOF-MS system (Figure 1b and Figure S1b in the Supporting Information) is described elsewhere.[27−29] In brief, 355 nm pulses (25 mJ pulse energy, 10 Hz repetition rate, 5 ns pulse width) from a Nd:YAG laser (Surelite III, Continuum Inc., Santa Clara, USA) were used to generate vacuum ultraviolet photons (118 nm, 10.5 eV) by third harmonic generation (THG) in a xenon-filled gas cell (Xe 4.0, 12 mbar).[30] The difference in refractive indices of 355 and 118 mm light in the MgF_2-lens of the apparatus was used to separate the VUV light from the primary UV beam. Only the VUV light was focused in the ion source for single-photon ionization (SPI) of the analytes in the effusive molecular beam of the inlet system of the modified TOF mass spectrometer (Kaesdorf Instrumente für Forschung and Industrie, München, Germany). By using two PC transient recorder boards (Aquiris, Switzerland, 250 MHz, 1 GS s^{-1}, 128 kb) to acquire the mass spectra, a dynamic range of ~5 orders of magnitude was achieved.[28] A mass range of 5 to 300 m/z was recorded at 10 Hz by using purposely written acquisition software (LabView, National Instruments, Austin, USA). The mass spectral peak intensities in the SPI mass spectra were normalized to the nitrogen peak (28 m/z), which is inherently produced from the constant nitrogen fraction in the sampling flux by residual electron ionization (EI). The residual EI is caused by electrons emitted from metal parts in the ion source hit by VUV stray photons (photo effect), which subsequently are accelerated in the electrostatic ion extraction field.[29]

In the present study, standardized scientific research reference cigarettes (3R4F, ISO tar-yield 9.3 mg, University of Kentucky, USA)[31,32] were used. Prior to the experiments, the 3R4F cigarettes were stored at 22 °C in an air-conditioned laboratory. The cigarettes were lit by an electrical lighter (Borgwaldt KC, Hamburg, Germany) and smoked according to the ISO-3308 protocol[17] (one bell-shaped puff of 2 s duration and 35 mL volume every 60 s) by a single-port smoking machine (LM1, Borgwaldt KC, Hamburg, Germany). The average linear burning rate of the cigarette was determined to be 9 ± 0.2 mm/s (during puff) and 0.10 ± 0.02 mm/s (during smoldering) by digital video monitoring (4 replicates).[25] On the basis of this information, the starting position of the paper burn line of the third puff in ISO smoking of 3R4F cigarettes was defined to be 1.30 cm behind the burning-tip end of the cigarette.

For this study, the third puff was investigated, because the burning tip of the cigarette, referred to as the "coal", is more reproducibly established in the third puff than in the earlier two

DOI: 10.1021/ac503512a
Anal. Chem. 2015, 87, 1711−1717

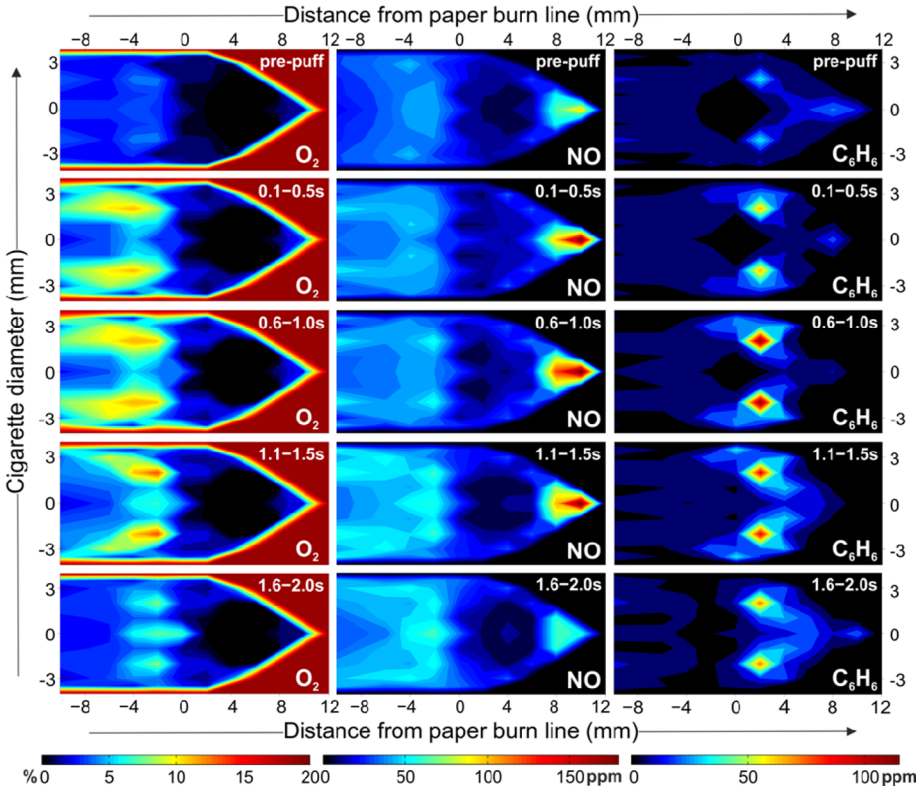

Figure 3. Time evolution of the quantitative substance concentration maps for O_2, NO, and C_6H_6 in the cigarette tip/ash cone before and during the third puff (ISO) of a 3R4F research cigarette in 500 ms averages. The first row depicts the prepuff situation. The following four rows show the situation in the first, second, third, and last quarter of the 2 s lasting puff.

puffs. In the following experiments, the position of the paper burn line during the beginning of the third puff (highest flow rate) was defined as the ±0 position. For each experiment, the μ-probe-sampling capillary is inserted perpendicular into the cigarette rod at a preset sampling position and depth. Combustion and pyrolysis gases are extracted while the ember front (paper burning line) is moving over the probe position.

An obtained averaged SPI-MS mass spectrum (3rd puff) of a selected individual measurement is exemplarily shown for one sampling point in Figure 1d. Some compounds in the soft SPI-MS mass spectrum are assigned according to previous studies.[22,23] In Figure 1c, the course of the NO and benzene concentrations over the lapse of the third puff are depicted. Similar measurements were done for the 40 different sampling positions (i.e., different positions along the cigarette rod length in the x-direction and injection depths in the y-direction) and depicted in Figure 2a. An accurate positioning system (see Figure S1a,c in the Supporting Information) and high reproducibility of the machine smoking process enabled us to obtain technical replicate mass spectrometric measurements at each position. For each measurement point and replicate, a time series of 1400 mass spectra were acquired to allow analysis of the relative peak intensity over time. After removing outliers (Grubbs test, 95% confidence interval) caused, e.g., by capillary blocking incidents, 4−5 of the technical replicates for each μ-probe position were averaged by using Excel 2007 (Microsoft, Redmond, USA). Primary data analysis (time-average of every five consecutive single mass spectra recorded with a frequency of 10 Hz, yielding a time resolution of 2 Hz) was performed via Origin software (Version 7.5 Origin Lab, Northampton, USA). The collected averaged data from the different sampling points were combined to quantitative chemical maps, showing the spatial distribution of the species concentrations for a given time. The software package Matlab (The MathWorks, Natick, USA) was used for construction of the spatial concentration-distribution maps of O_2, NO, and C_6H_6 (Figures 2d,e,f and 3), in addition to a video showing changes in the chemical distribution maps animated with time (movie in the Supporting Information).

Owing to the rotational symmetry of the cigarette, the observed substance abundances can be mirrored at a vertical mirror plane along the cigarette middle axis (Figure 2g). In Figure 2b, the estimated thermal distribution map adapted from literature values for the peak maximum temperatures[33] are given. In Figure 2c, the approximated differential gas flow field (after ref 34) in the cigarette during the middle of the puff is shown. The position-resolved abundance maps (Figures 2d,e,f and 3) were generated by taking abundance data from all measurement positions at a given time point relative to the zero position of the progressing paper burn line (=middle or maximum flow position of the third ISO puff). The concentrations of benzene (C_6H_6) and nitrogen oxide (NO) were quantified by an external standardization procedure using 10 ppm of C_6H_6 and NO reference gas standards. Oxygen (O_2) was quantified on the basis of the O_2 signal in air (the time-resolved data shown in Figure 3, first column). Note that the position of the PBL in the middle of the third puff was assigned as the distance =0 (zero distance) to provide a reference point for other positions (Figures 2a−f and 3 and movie in the Supporting Information).

DOI: 10.1021/ac503512a
Anal. Chem. 2015, 87, 1711−1717

RESULTS AND DISCUSSION

In Figure 2d–f, the chemical concentration maps of the compounds oxygen (O_2, m/z 32, ionized by residual electron ionization),[29] nitrogen monoxide (NO, m/z 30), and benzene (C_6H_6, m/z 78) in the middle of the third puff are shown (for the visualization of the time interval, see Figure 1c red shaded region). As the paper burn line (PBL) position is very reproducible for the different smoking experiments, all maps are labeled with respect to the position of PBL during the middle of the third puff.

It is obvious that the chemical concentration maps of the selected compounds are very different. The oxygen map (Figure 2d) depicts that in the tapered ash cone O_2 is nearly depleted owing to char oxidation processes.[35] This region is also characterized by the highest temperatures (Figure 2b), although the flow vectors (Figure 2c) show that the gas velocity in the ash cone itself is comparably low. The entering of air into the cigarette rod close to the PBL (Figure2d, indicated by blue arrows) leads to clearly visible increased O_2 concentrations behind the PBL. The benzene concentration (Figure 2e) is peaking in the rear part of the O_2-depleted zone. This is a region of intense combustion and pyrolysis reactions at high temperatures: C_6H_6 can be formed by pyrolysis of the residual char in the ash cone or by gas phase combustion reactions from unsaturated molecular and radical precursors.[36] In the benzene-rich zone, many other hydrocarbons such as 1,3-butadiene and toluene are abundant and can be seen in the bottom mass spectra in Figure S2 (Supporting Information). The abundance distribution of NO (Figure 2f) shows a strikingly different signature. The highest concentrations of NO are observed at the tip of the ash cone.

Figure 3 shows the evolution of chemical concentration maps of oxygen, benzene, and nitrogen monoxide recorded during the progress of the puff in 0.5 s time intervals (prepuff and first to forth puff interval). Before the puff is started (Figure 3, first row, top panel), the cigarette is in steady-state smoldering. A residual diffusive flow of O_2 owing to its concentration gradient at the PBL is observed. Small concentrations of C_6H_6 (and many other hydrocarbons, not shown here) are observed slightly before the PBL. NO is present in the highest concentration at the tip of the ash cone. The concentration of other hydrocarbons is relatively low there, although a small amount of C_6H_6 is present (owing to combustion of residual char). At the onset of the puff, the forced air in-flow becomes clearly visible in the O_2 map (Figure 3, second row, first 0.5 s of the puff). As a consequence, the spatial-dimension of the NO and C_6H_6 formation zones and the compound concentrations are rising.

With further increase of the puff flow (Figure 3, third row, second 0.5 s of the puff), the peak concentrations of C_6H_6 and NO are increased as well. Their respective formation zones are expanded partially in the downstream direction. A very similar pattern is observed in the concentration distribution maps of the third 0.5 s of the puff (Figure 3, fourth row). The profiles according to the fourth and last 0.5 s of the puff are depicted in the fifth row of Figure 3. If the C_6H_6 formation zone is compared with that of the first 0.5 s, an extension in the opposite direction of the puff flow is observed with slightly higher peak concentrations. This is the effect of the elevated char temperatures (char combustion) in the ash cone during and after the puff.

The observed concentration distributions for the three selected species were highly dynamic and can be interpreted as follows. Although the exact mechanism of NO formation during solid fuel combustion is not fully understood, basic theories are available and can be compared with the observed substance pattern.[37] Fuel bound nitrogen is the major source of NO from tobacco combustion, as the temperatures stay below 1000 °C, which excludes the Zeld'ovich- or prompt-NO formation mechanism. As the gases move downstream from the tip of the ash cone, however, the concentration of organic molecules and radicals increase, as observed for C_6H_6 (and many other organics, see Figure S2, bottom part, Supporting Information). This causes a reduction in NO abundance owing to the so-called "reburn mechanism",[38] in which NO reacts with, for example, the HCCO radical to form HCNO + CO or HCN+ CO_2. HCNO and HCN are subsequently converted to nitrogen. In this fuel-rich reburn zone, the formed organic nitrogen species are mostly reduced to elemental nitrogen as well. The pattern of NO formation observed within a cigarette reflects the situation of a staged combustion setup for minimizing NO_x formation in engineering combustion systems such as coal dust burners. The high NO_x concentrations from the primary and secondary combustion, which in engineering combustion can be due to both fuel- and thermal-NO_x formation mechanisms, are reduced by injecting additional fuel in the reburn zone. The air influx around the PBL also is postcombusting much of the pyrolysis gases. This step resembles the so-called tertiary combustion zone in engineering combustion systems.

In conclusion, this experiment reveals for the first time that the observed chemical concentration maps of NO and C_6H_6 in the middle of a cigarette puff closely correspond to the known formation and destruction behavior of NO during combustion processes. Formation of NO, however, is slightly decreased in comparison to the first 0.5 s of the puff. The sequences in Figure 3 reflect detailed mechanisms of the chemical formation of these species with good time and spatial resolution under the dynamic forced flow. In Figure 4a, the relevant NO formation and destruction processes are given in a simplified scheme and the respective formation and destruction regions are indicated.

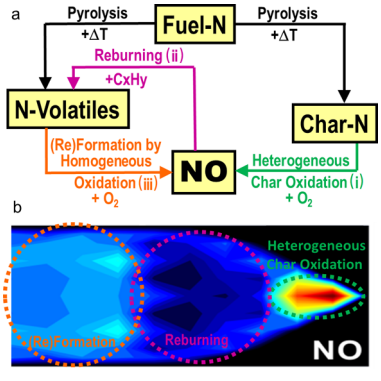

Figure 4. NO formation and destruction in the burning cigarette. (a) Simplified scheme of the relevant NO formation and destruction mechanisms (i) heterogeneous char oxidation (NO formation), (ii) NO reburn by homogeneous reaction with organic species/radicals (NO destruction), and (iii) homogeneous gas phase oxidation of N volatiles (reformation via HCN). (b) Distribution map of NO during the middle of the third puff with indicated NO formation/destruction regions i, ii, and iii.

DOI: 10.1021/ac503512a
Anal. Chem. 2015, 87, 1711−1717

The NO concentration map depicting the situation in the middle of the puff (Figure 4b) visualizes the occurrence of these pathways during tobacco burning. The dynamic changes in the generated concentration distribution maps during the 2 s puff can also be used to generate an animated movie clip, showing the dynamical changes in "real time" (movie in the Supporting Information).

The spatially resolved concentration data together with the gas flow vector data (Figure 2c) in the cigarette also allows one to estimate the effective concentration change rates $\Delta c/\Delta t$ (i.e., the net destruction/formation kinetics of the analyzed compounds) at a given time t of the puff. Especially in the middle of the puff, gas volume elements are drawn quite fast through the cigarette rod (at tip of the ash cone with 5−8 mm/s). Thus, the concentration changes along the flow path can be associated with the effective net destruction/formation rates. This approach makes use of the approximation that finite volume elements are displaced through the cigarette rod with the direction and speed(s) of the flow vectors (see Figure 2c). If suddenly all chemical reactions would stop, these finite elements would travel along the flow paths with unchanged concentrations.

The observed spatial concentration changes in the cigarette could be translated in concentration change rates $\Delta c/\Delta t$ by differentiating the change of the concentration (Δc) over the transport distance ($\Delta x = \Delta v \cdot \Delta t$). This is demonstrated for NO and C_6H_6 along the axial center line of the tobacco rod for the time frame of 1.1 to 1.4 s after puff start. In Figure 5a, the measured concentrations of NO and C_6H_6 (Figure 5a) along the center line of the cigarette rod are depicted as a function of the PBL position x. The estimated linear flow speed (mm/s) as a function of the PBL position x from the flow simulation literature data[34] is shown in Figure 5b. In Figure 5c, the calculated effective net destruction/formation rates for benzene and nitrogen monoxide are depicted ($\Delta c/\Delta t$ in ppm/s). In principle, any other flow path through the interior of the cigarette rod can be calculated and depicted in a similar way.

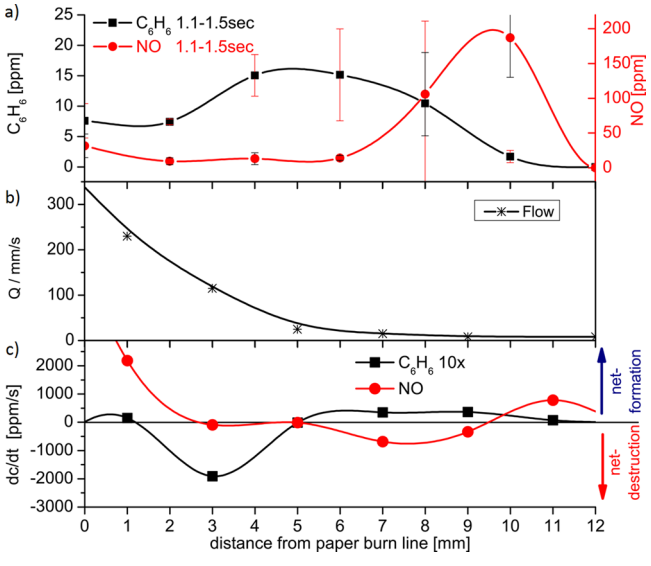

Figure 5. Concentration profiles and effective formation/destruction kinetics of NO and C_6H_6 along the central line of the cigarette in the ash cone during the maximum flow of the third puff (ISO) of a 3R4F research cigarette. (a) Concentrations (ppm) of NO and C_6H_6 along the central line of the cigarette in the ash cone with error bars (standard deviation). (b) Linear flow (mm/s) rate along the central line of the cigarette in the ash cone during the maximum flow of the third puff. (c) Effective formation/destruction rates ($\Delta c/\Delta t$ in units of ppm/s) of NO and C_6H_6.

This method may give kinetic data on solid fuel combustion for fundamental combustion chemistry studies. It is important to notice that the technique is not limited to analyze cigarette combustion, although this test case has provided a particularly interesting and relevant example. However, as cigarette smoking machines are well developed test devices with very good stability, which are ensuring reproducible combustion conditions, they might be used for other combustion studies as well. Cigarette paper reels filled with any kind of ground combustible material such as coal, lignite, peat, wood, or other biomass might be used as study objects. The microprobe−photoionization mass spectrometry approach could be adapted for studying many other solid−gas phase boundary layer-based reactions such as fuel or biomass systems under smoldering or flaming combustion. Further, the positionally resolved analysis of heterogeneous catalytic reactions could be an interesting application field. For larger combustible solid feedstock materials, the μ-probe also may be inserted via a drilled channel into the interior region to study the internal release of combustible pyrolysis gases in cracks and fissures as well as the formation of combustion products. This would be a similar approach as the previously reported analysis of roast gases from individual coffee beans during roasting.[39,40]

CONCLUSION

By using a μ-probe sampling technique combined with soft laser-based photoionization mass spectrometry (SPI-TOF-MS, Figure 1), we have demonstrated time-resolved two-dimensional mapping of the quantitative molecular abundance distributions of individual chemical species in the highly dynamic and heterogeneous combustion process of a burning cigarette. The time-resolved concentration patterns can be displayed in an animated movie, showing the progression of the changes over time (see movie in the Supporting Information). From the numerous chemical species accessible, O_2, NO, and C_6H_6 have been selected to demonstrate the possible insights with this technique regarding thermochemical species formation and destruction in different zones of the cigarette modulated by defined patterns of air influx (Figures 2 and 3). The observed concentration patterns are sound and in good agreement with the formation[41] and destruction[38] chemistry of NO combustion pyrolysis systems (Figure 4). Furthermore, a kinetic analysis along the central line of the cigarette rod has enabled us to determine spatially resolved destruction and formation rates (Figure 5). The presented microprobe sampling−photoionization mass spectrometry approach for time and space resolved quantitative chemical profiling and mapping is feasible for multiple applications, e.g., in combustion chemistry or heterogeneous catalysis research.

ASSOCIATED CONTENT

Supporting Information

Additional information as noted in text. This material is available free of charge via the Internet at http://pubs.acs.org.

AUTHOR INFORMATION

Corresponding Author

*E-mail: ralf.zimmerman@uni-rostock.de.

DOI: 10.1021/ac503512a
Anal. Chem. 2015, 87, 1711−1717

Notes

The authors declare no competing financial interest.
[#]R.B.: Deceased.

REFERENCES

(1) D'Anna, A. *Proc. Combust. Inst.* **2009**, *32*, 593−613.
(2) Demirbas, A. *Prog. Energy Combust. Sci.* **2007**, *33*, 1−18.
(3) Solomon, P. R.; Serio, M. A.; Suuberg, E. M. *Prog. Energy Combust. Sci.* **1992**, *18*, 133−220.
(4) Uchimura, T.; Imasaka, T. *Anal. Chem.* **2000**, *72*, 2648−2652.
(5) Weickhardt, C.; Boesl, U.; Schlag, E. W. *Anal. Chem.* **1994**, *66*, 1062−1069.
(6) Appel, J.; Bockhorn, H.; Frenklach, M. *Combust. Flame* **2000**, *121*, 122−136.
(7) Pelce, P.; Clavin, P. *J. Fluid Mech.* **1982**, *124*, 219−237.
(8) Northway, M. J.; Jayne, J. T.; Toohey, D. W.; Canagaratna, M. R.; Trimborn, A.; Akiyama, K. I.; Shimono, A.; Jimenez, J. L.; DeCarlo, P. F.; Wilson, K. R.; Worsnop, D. R. *Aerosol Sci. Technol.* **2007**, *41*, 828−839.
(9) Skjøth-Rasmussen, M. S.; Glarborg, P.; Østberg, M.; Johannessen, J. T.; Livbjerg, H.; Jensen, A. D.; Christensen, T. S. *Combust. Flame* **2004**, *136*, 91−128.
(10) Taatjes, C. A.; Hansen, N.; Osborn, D. L.; Kohse-Höinghaus, K.; Cool, T. A.; Westmoreland, P. R. *Phys. Chem. Chem. Phys.* **2008**, *10*, 20−34.
(11) Vattulainen, J.; Nummela, V.; Hernberg, R.; Kytola, J. *Meas. Sci. Technol.* **2000**, *11*, 103−119.
(12) Baker, R. R. *Nature* **1976**, *264*, 167−169.
(13) Heger, H. J.; Zimmermann, R.; Dorfner, R.; Beckmann, M.; Griebel, H.; Kettrup, A.; Boesl, U. *Anal. Chem.* **1999**, *71*, 46−57.
(14) Streibel, T.; Hafner, K.; Mühlberger, F.; Adam, T.; Warnecke, R.; Zimmermann, R. *Anal. Bioanal. Chem.* **2006**, *384*, 1096−1106.
(15) A Report of the Surgeon General: How Tobacco Smoke Causes Disease...What It Means to You; 2010; http://www.cdc.gov/tobacco/data_statistics/sgr/2010/consumer_booklet/pdfs/consumer.pdf.
(16) Stratton, K. *Tob. Control* **2001**, *10*, 189.
(17) *Routine analytical cigarette-smoking machine -- Definitions and standard conditions*; ISO 3308:1991; International Organization for Standardization: Geneva, 1991.
(18) Chen, P. X.; Moldoveanu, S. C. *Beitr. Tabakforsch. Int.* **2003**, *20*, 448−458.
(19) Baker, R. *J. Anal. Appl. Pyrolysis* **1987**, *11*, 555−573.
(20) Borgerding, M.; Klus, H. *Exp. Toxicol. Pathol.* **2005**, *57*, 43−73.
(21) Baker, R. R. *Prog. Energy Combust. Sci.* **1981**, *7*, 135−153.
(22) Adam, T.; Mitschke, S.; Baker, R. R. *Beitr. Tabakforsch. Int.* **2009**, *23*, 203−226.
(23) Eschner, M. S.; Selmani, I.; Gröger, T. M.; Zimmermann, R. *Anal. Chem.* **2011**, *83*, 6619−6627.
(24) Hanley, L.; Zimmermann, R. *Anal. Chem.* **2009**, *81*, 4174−4182.
(25) Hertz, R.; Streibel, T.; Liu, C.; McAdam, K. G.; Zimmermann, R. *Anal. Chim. Acta* **2012**, *714*, 104−113.
(26) Sundstrom, D. W.; Demichie, R. L. *Exp. Eng. Chem. Process Des. Dev.* **1971**, *10*, 114−122.
(27) Adam, T.; McAughey, J.; McGrath, C.; Mocker, C.; Zimmermann, R. *Anal. Bioanal. Chem.* **2009**, *394*, 1193−1203.
(28) Mitschke, S.; Adam, T.; Streibel, T.; Baker, R. R.; Zimmermann, R. *Anal. Chem.* **2005**, *77*, 2288−2296.
(29) Mühlberger, F.; Hafner, K.; Kaesdorf, S.; Ferge, T.; Zimmermann, R. *Anal. Chem.* **2004**, *76*, 6753−6764.
(30) L'Huillier, A.; Balcou, P.; Candel, S.; Schafer, K. J.; Kulander, K. C. *Phys. Rev. A* **1992**, *46*, 2778−2790.
(31) Intorp, M.; Purkis, S. *Beitr. Tabakforsch. Int.* **2011**, *24*, 174−186.
(32) Intorp, M.; Purkis, S.; Wagstaff, W. *Beitr. Tabakforsch. Int.* **2011**, *24*, 243−251.
(33) Baker, R. R. *High Temp. Sci.* **1975**, *7*, 236−247.
(34) Saidi, M. S.; Hajaligol, M. R.; Rasouli, F. *J. Anal. Appl. Pyrolysis* **2004**, *72*, 141−152.
(35) Baker, R. R. *Beitr. Tabakforsch. Int.* **1981**, *11*, 1−17.
(36) Kinoshita, C. M.; Wang, Y.; Zhou, J. *J. Anal. Appl. Pyrolysis* **1994**, *29*, 169−181.
(37) Glarborg, P.; Jensen, A. D.; Johnsson, J. E. *Prog. Energy Combust. Sci.* **2003**, *29*, 89−113.
(38) Glarborg, P.; Kristensen, P. G.; Dam-Johansen, K.; Alzueta, M. U.; Millera, A.; Bilbao, R. *Energy Fuels* **2000**, *14*, 828−838.
(39) Hertz-Schünemann, R.; Dorfner, R.; Yeretzian, C.; Streibel, T.; Zimmermann, R. *J. Mass Spectrom.* **2013**, *48*, 1253−1265.
(40) Hertz-Schünemann, R.; Streibel, T.; Ehlert, S.; Zimmermann, R. *Anal. Bioanal. Chem.* **2013**, *405*, 7083−7096.
(41) Molina, A.; Eddings, E. G.; Pershing, D. W.; Sarofim, A. F. *Prog. Energy Combust. Sci.* **2000**, *26*, 507−531.

DOI: 10.1021/ac503512a
Anal. Chem. 2015, 87, 1711−1717